

Time reversal symmetry breaking and zero magnetic field Josephson diode effect in Dirac semimetal Cd₃As₂-mediated asymmetric SQUIDs

W. Yu¹, J.J. Cuozzo², K. Sapkota¹, E. Rossi³, D.X. Rademacher¹, T.M. Nenoff¹, W. Pan²

¹ Sandia National Labs, Albuquerque, NM 87185, USA

² Sandia National Labs, Livermore, CA 94551, USA

³ Department of Physics, College of William and Mary, VA 23187, USA

Abstract

A *zero-magnetic-field* Josephson diode effect (JDE) is observed in an asymmetric superconducting quantum interference device (SQUID) mediated by Dirac semimetal Cd₃As₂. Herein it is shown that phase coupling between the surface and bulk superconducting channels, a unique phenomenon recently identified in the observations of fractional Josephson effect and Leggett modes in Cd₃As₂, can break time reversal symmetry (TRS) and, therefore, give rise to the zero-field JDE. It is identified that the efficiency of the JDE can be readily controlled by varying the geometry of the Josephson junction (JJ) arms in the SQUIDs, thus providing an explanation of different JDE behaviors in two SQUIDs examined in this work. Our results are anticipated to have important implications in superconducting electronic circuit applications.

The diode effect in a p-n junction plays an important role in modern microelectronics. Due to broken inversion symmetry between the electron (n) and hole (p) doped regimes, electronic transport is non-reciprocal, i.e., electrical current can flow only in one direction. This non-reciprocal nature has been widely utilized in electronic devices such as transistors, light-emitting diodes, solar cells, etc.

Recently, a similar diode effect has attracted a great deal of interest in superconducting systems [1-62]. Like the diode effect in the p-n junctions, the superconducting diode effect (SDE), or specifically the Josephson diode effect (JDE) in Josephson junctions (JJs), is expected to find important applications such as passive on-chip gyrators and circulators. Such devices would be particularly impactful in quantum computing applications [63]. Moreover, the SDE/JDE can be utilized as an alternative method to study novel superconductor properties, such as finite momentum Cooper pairing [2,10].

In a typical JJ or superconducting quantum interference device (SQUID), the I-V curve is linear in the high current regime where the device is in the normal state, see Figure 1d. The voltage V_{dc} drops abruptly to zero at the so-called retrapping current I_{+r} (for the current sweeping down) and stays at zero over a large current range until a switching current $-I_c$ is reached. Herein, we take this switching current as the critical current (I_c) of the JJ and use the terminology of critical current throughout in the paper. Beyond $-I_c$, the I-V curve becomes linear, and the device enters the normal state again. For the current sweeping up curve, a similar shape in the I-V curve is observed, and the positions of corresponding $-I_r$ and I_{+c} are marked. In general, $I_{+c} = I_c$, independent of current sweeping directions as long as either time reversal symmetry (TRS) or inversion symmetry is present. However, when both symmetries are broken, the critical current can display different values depending on which direction the current is swept, a phenomenon called the JDE [1,2]. Inversion symmetry is broken in non-centrosymmetric superconducting systems or in device structures such as asymmetric SQUIDs as we will discuss in this work. However, superconductors with intrinsic broken TRS are rare because superconducting condensates are typically formed by pairs of electrons related by TRS. Consequently, external magnetic (B) fields [3] or magnetic heterostructures [4,5] are exploited to break TRS. In this

regard, it is surprising that in recent experiments the JDE was observed at zero B field in non-magnetic materials [6,7,62], thus calling for more investigations into Josephson junctions made of topological quantum materials [64] where non-trivial band topology and topological superconductivity are shown to facilitate the JDE [9-19].

In this paper, we demonstrate JDE in two asymmetric SQUIDs made of Dirac semimetal [65,66] Cd₃As₂, see Fig. 1. In SQUID1, the efficiency η_c of JDE, defined by $\eta_c = (I_{+c} - I_{-c}) / (I_{+c} + I_{-c})$, is very weak and essentially zero at zero B field. It becomes finite at finite B fields. In SQUID2, surprisingly, a large JDE is observed at zero B field, with an efficiency of $\sim 9\%$. Our analysis based on the resistively shunted junction model suggests that a definitive phase coupling between the surface and bulk superconducting channels can break TRS at zero B field. This, together with the geometric difference in the two JJ arms in asymmetric SQUIDs, is responsible for the observation of the zero B field JDE. Furthermore, our theoretical simulation shows that η_c depends on the geometry of SQUIDs, thus providing an explanation of non-observation of zero-field JDE in SQUID1.

Figs. 1a and 1b shows the scanning electron microscope images of the two SQUIDs we studied in this work [see the Supplemental Material (SM) for details [67]]. For electronic measurements, the devices are cool-down and emersed in a cryogenic liquid at a temperature of ~ 0.2 or 0.03 K, well below the proximity-effect induced and Al superconducting transition temperatures.

SQUID1 Results. I-V curves measured in SQUID1 at $T = 0.2$ K at $B = 0$ and 16 mT are shown in Fig. 1c and Fig. 1d, respectively. In both cases, current is swept first from $-7 \mu\text{A}$ to $+7 \mu\text{A}$ and then from $+7 \mu\text{A}$ to $-7 \mu\text{A}$. Multiple switching behavior is observed for both I_c and I_r , see inset of Fig. 1c. Here, we use the first switching position to define I_c and I_r . This multiple switching behavior is suppressed under a finite B field, for example, at 16 mT (Fig. 1d). Moreover, at $B = 0$, the current up and down traces overlap almost perfectly (barring the multiple switching events), and I_c and I_r are close to each other for either current direction. However, at a

finite B field, e.g. $B = 16$ mT, I_c and I_r differ considerably in the same current sweeping trace. For example, $I_{+r} = 3.8 \mu\text{A}$, while $I_{-c} = 5.82 \mu\text{A}$ in the current sweeping down trace.

Differential resistance dV/dI [67] is measured together with the I-V curves. The 2D color plots of dV/dI in SQUID1 as a function of DC current and B field for current sweeping up and down are shown in Figures 2a and 2b, respectively. The uniformly colored blue area in the middle represents the proximity [68] induced supercurrent regime [69-73], and the sharp edge of the region highlights the value of I_c (as well as I_r). The B field dependence of I_c (as well as I_r) contrasts with the typical oscillatory pattern expected in a conventional SQUID where I_c oscillates with the B fields with a period inversely proportional to the area of the SQUID ring. Instead, $I_{\pm c}$ (as well as $I_{\pm r}$) displays a non-oscillatory, non-monotonic magnetic field dependence. Starting from $B = 0$, $I_{\pm c}$ and $I_{\pm r}$ first increase with increasing magnetic field strength, reach a maximal value which depends on the current sweep direction, and then decrease with further increasing magnetic fields. Eventually, both $I_{\pm c}$ and $I_{\pm r}$ become zero when the B field reaches the critical magnetic field ($\sim \pm 35$ mT [69]) of the superconducting Al thin film, at which the proximity effect disappears. The enhancement of $I_{\pm c}$ with B around the zero field is strikingly large, it reaches 214% of its zero-field value at $B \sim 11-12$ mT. We notice here that, interestingly, this maximum enhancement is similar to what is reported in Ref. [74]. The large increase in I_c is dramatically different from that in a single JJ also made of Cd_3As_2 where the maximal enhancement was merely 4% [69]. On the other hand, we notice that similar magnetic field response of I_c (and I_r) was also observed [19,75-77] in the past in JJs with broken TRS and was attributed to the existence of two supercurrents that are out of phase with each other [19]. The same mechanism should also be responsible for the observed magnetic field response in our device.

Magnetic field responses of I_{+c} and $-I_{-c}$ are plotted for SQUID1 in Figure 2c. The efficiency of I_c JDE η_c is plotted in Figures 2d. At $B = 0$, η_c is very weak and essentially zero. As B increases, η_c becomes finite and displays an even function of B field dependence around $B = 0$. At high B fields in the negative and positive directions, different B-dependent behaviors are observed. In

the negative B field regime, η_c saturates to a value of $\sim 2.5\%$ beyond -5 mT. On the other hand, in the positive B field regime, after reaches a local maximum of $\sim 2.5\%$ at $B \sim 5$ mT, η_c starts decreasing, and becomes negative for $B > 10$ mT. The magnitude of η_c continues to increase beyond ~ 20 mT when the differential resistance become non-zero over the whole DC current range, as indicated by the color change in Figs. 2a and 2b. Overall, η_c displays a diode-like behavior with the B field. This might be due to the interplay of an external magnetic field and the possible spontaneous breaking of time-reversal symmetry in Al-Cd₃As₂ heterostructures, but its exact origin is presently not known.

The B field dependence of retrapping current (I_{+r} and $-I_{-r}$) and its efficiency $\eta_r = (I_{+r}-I_{-r})/(I_{+r} + I_{-r})$ are shown in Figures 2e and 2f, respectively. η_r also shows a diode-like behavior with the B field. $\eta_r \sim 0$ between $B = -20$ and $B = 10$ mT, and then becomes finite and increases with increasing B fields. I_r depends on the dissipative current in the normal state. Non-reciprocal I_r represents another aspect of the JDE and has also been observed in recent experiments [5, 10, 49]. It has been shown that in the dissipative regime in the presence of a strong spin-orbit coupling, which is known to exist in Cd₃As₂, $I_{+r} \neq I_{-r}$ can occur [1]. It is interesting that both η_c and η_r follow a similar diode-like behavior with the B fields. Future studies will be focused on understanding this apparent correlation.

SQUID2 Results. In this SQUID, a large *magnetic-field-free* JDE is observed. The I-V curves at $B = 0$ T for DC currents sweeping up and sweeping down are shown in Figure 3a. For the trace of current swept down from $6 \mu\text{A}$ to $-6 \mu\text{A}$, $I_{-c} = 2.99 \mu\text{A}$. For the trace of current sweeping up, $I_{+c} = 3.62 \mu\text{A}$. This value is significantly larger than I_{-c} ($I_{+c} - I_{-c} = 0.63 \mu\text{A}$) and the corresponding JDE efficiency $\eta_c = (I_{+c}-I_{-c})/(I_{+c}+I_{-c}) = 9.5\%$, demonstrating a large magnetic-field-free JDE in SQUID2. Like in SQUID1, there are multiple retrapping events, such as the one at $-3.02 \mu\text{A}$ and the other at $-2.93 \mu\text{A}$ in the sweeping up trace. A large JDE is again observed in the I-V data taken at $B = 6$ mT, see Figure 3b: $I_{+c} = 4.19 \mu\text{A}$ and $I_{-c} = 3.50 \mu\text{A}$. Consequently, $I_{+c} - I_{-c} = 0.69 \mu\text{A}$ and $\eta_c = 9.0\%$. These values are close to those at $B = 0$. No diode effect is observed in I_r , though. At $B = 0$, I_{+r} and I_{-r} appear to be equal, $\sim 3 \mu\text{A}$.

Differential resistance in SQUID2 at $T = 30$ mK as a function of I_{dc} and B field is plotted for both current sweeping up and down traces in Fig. 4a and Fig. 4b, respectively. We note here that for the sweeping down traces, the current stops at $I_{dc} = 0$. Consequently, information on I_c is not available. There are several features worth pointing out. First, the non-monotonic B field dependence of the critical current is also seen in SQUID2, as in SQUID1. At $B = 0$, $I_{+c} = 4 \mu\text{A}$ and it increases with increasing B fields and reaches a maximal value of $\sim 5 \mu\text{A}$ at $B = 9$ mT. I_{+c} then decreases with B further increased. Second, $I_{\pm r}$ also shows a magnetic field-induced enhancement. Third, there are re-entrant supercurrent states at high B fields (see more data in the SM [67]).

In Fig. 4c, I_r , I_{+r} and $\Delta I_r = I_{+r} - I_r$ are plotted as a function of magnetic field. Unlike in SQUID1 where ΔI_r shows a monotonic B field dependence, ΔI_r in SQUID2 shows a much richer B field dependent behavior. At zero and small positive B fields, I_{+r} and I_r are equal, $\Delta I_r = 0$. This reciprocal behavior persists up to 10mT. Between 10 and 17 mT, I_{+r} and I_r generally differ from each other and $\Delta I_r \neq 0$, except at $B = 12$ mT, when ΔI_r quickly drops to zero. ΔI_r assumes a negative value between 17 and ~ 26 mT, in which there are no supercurrent states, before returning to zero again at $B > 26$ mT when the device enters the reentrant supercurrents regime.

The observation of a zero-B field JDE in SQUID2 is striking, as Cd_3As_2 itself is non-magnetic. In the following, we first argue that mechanisms, such as the Meissner [61] and circuit inductance effects [78], cannot be responsible for the JDE observed in our Cd_3As_2 SQUIDs. Next, we propose a time-reversal-symmetry breaking mechanism to be responsible for the existence of the zero-magnetic field JDE.

Recently, the Meissner effect was shown to play an important role in the magnetic field induced diode effect [61]. However, this effect cannot account for the JDE in our Cd_3As_2 SQUIDs. As shown in Fig. 2d, η_c in SQUID1 displays an even function of the B fields around $B = 0$ for the

positive and negative B fields. This is very different from the Meissner effect induced SDE, where the efficiency is an odd function of the B fields [61].

Time reversal symmetry requires $I_{+c}(+B) = |-I_{-c}(-B)|$. Therefore, as long as the SQUID does not break time reversal symmetry, no diode effect can be present even when inductance effects are taken into account, as discussed in [78,79]. In the SM [67], we provide a detailed theoretical calculation explicitly showing that even in the dynamical regime, when inductance effects are expected to be more relevant, the voltage-current (V-I) characteristic is symmetric when $B=0$, and its asymmetry is odd with respect to B when B is not zero, as required when the system does not spontaneously break time reversal symmetry.

To unravel the origin of the JDE observed in our SQUIDs, we first identify sources of broken inversion symmetry. Microscopically, the surface states in Dirac semimetal Cd_3As_2 have broken inversion symmetry in both the junctions of SQUID1 and SQUID2 owing to the termination of the crystal lattice. Apart from microscopic details, differences in the geometries of the JJ arms of our SQUIDs can further cause asymmetries in, such as, the sinusoidal form of the current phase relationship (CPR), self-inductances, I_c , and R_n (normal state resistance). However, none of the materials forming the SQUIDs have to be non-centrosymmetric for the presence of a diode effect. An asymmetry between the transparency of the superconducting channels carrying the current across the SQUID is sufficient, when time-reversal is broken, to explain the presence of a superconducting diode effect, as discussed in Refs. [20,21].

Second, we note that the finite B field JDE in SQUIDs was discussed previously [20,21]. There, JDE only appears under a finite magnetic field due to non-sinusoidal current-phase relations [20,21]. While this discussion is sufficient to understand JDE in our devices under an external magnetic field, the zero-field JDE observed in SQUID2 requires further elucidation. In the absence of an external magnetic field, TRS must be broken in another way to realize a JDE. We propose that the Josephson coupling between a conventional superconductor (i.e., aluminum) and a two-band superconductor (i.e., the surface and bulk superconducting channels in Cd_3As_2) as

well as the Josephson coupling between the surface and bulk states (as previously identified in Refs. [69] and [80]) can break TRS [81]. In our system superconducting correlations are induced in the bands (band 1 and 2) of Cd₃As₂ by the superconductivity in Al via the proximity effect. The coupling of band 1 and 2 to Al, a standard s-wave superconductor, favors order parameters in the two bands with no relative phase difference. Such “alignment” of the superconducting order parameters in the two bands can be frustrated if spin-orbit coupling favors pairing correlations in the two bands with a phase difference $\sim\pi$. This situation is analogous to the one of two-band superconductors with a negative inter-band Josephson coupling [81]. In these conditions the phases of the superconducting order parameters in band 1 and 2 will have a “canted” equilibrium configuration with the phase of the order parameter in band 1 $\theta_1=\pm\theta_0$ and the phase of the order parameter in band 2 $\theta_2=-(\pm\theta_0)$, with $0<\theta_0<\pi$. The two possible states form a time-reversed pair, with each state in the pair breaking TRS. In a JJ based on Al/ Cd₃As₂, as the one shown in Fig.5(a), when the left side and right side of the junction are in different states of the time-reversed pair, see Fig. 5(a), the junction breaks the overall time reversal symmetry. In this situation the equilibrium phase difference, $\Delta\theta$, between the left and right lead of the JJ is non-zero for both bands: $\Delta\theta_1=\pm 2\theta_0$, $\Delta\theta_2=-(\pm 2\theta_0)$. The value of θ_0 , and therefore of $\Delta\theta_i$, depends on the coupling between Al and Cd₃As₂. Details of the interface between Al and Cd₃As₂, and the width and thickness of the Al layer, affect such coupling and therefore the value of θ_0 . For SQUIDS for which the values of θ_0 in the two JJs are different a diode effect will be present even when no external magnetic field is present [82,83]. We expect that such configuration of phases might be realized in SQUID2 giving rise to the observed zero-field diode effect.

The fact that SQUID1 does not exhibit a diode effect in the absence of an external magnetic field can be due to the fact that for such SQUID, in the ground state, $\Delta\theta_1$ ($\Delta\theta_2$) is to good approximation the same in both JJs forming the SQUIDS. However, the lack of an observable zero-field JDE in SQUID1 is more likely due to the fact that in SQUID1 the two JJs have very different critical currents, causing the SQUID to qualitatively behave as a single Cd₃As₂ JJ [69]. In SQUID2 the lengths of Junction-1 and Junction-2 are roughly equal, ~ 170 vs. ~ 180 nm, and therefore I_{c1} and I_{c2} are relatively close to each other, whereas in SQUID1 the junction length of

Junction-1 is quite shorter, ~ 61 nm, than the length of Junction-2, ~ 153 nm so that $I_{c1} \gg I_{c2}$. The suppression of the diode effect for $I_{c1} \gg I_{c2}$ can be illustrated with a minimal model for an asymmetric SQUID diode [21]: $I_1 = I_{c1} \sin \varphi$; $I_2 = I_{c2} \sin \varphi + I'_{c2} \sin 2\varphi$. Generally, I'_{c2} is non-zero if TRS is broken and results in the JDE. The CPR of the SQUID in the absence of inductance is [21]

$$J(\phi) = \sqrt{I_{c1}^2 + I_{c2}^2 + 2I_{c1}I_{c2} \cos \widehat{\Phi} \sin \varphi + I'_{c2} \sin(2\varphi - \widetilde{\Phi})},$$

where $\widehat{\Phi} = 2\pi\Phi/\Phi_0$, $\widetilde{\Phi} = \widehat{\Phi} + 2\gamma$ and $\tan \gamma = \frac{I_{c1} - I_{c2}}{I_{c1} + I_{c2}} \tan \frac{\widehat{\Phi}}{2}$. In the limit $I_{c1} \gg I_{c2}$, $\widetilde{\Phi} \approx 0$ which suppresses the JDE. Fig. 5b shows the dependence of JDE efficiency, η , on the ratio I_{c2}/I_{c1} with a magnetic flux $\Phi_0/4$ threading the SQUID ring. It is clearly seen that η is almost zero if $I_{c2}/I_{c1} \sim 0.1$ and reaches a maximal value for $I_{c2} \sim I_{c1}$.

In conclusion, our combined experimental and theoretical analysis demonstrate that the coupling of the superconducting phases between the surface and bulk states can break TRS and induce a zero-magnetic-field JDE in topological SQUIDs made of Dirac semimetal Cd_3As_2 . Importantly, by utilizing this unique property and the geometry of SQUIDs, one can control the efficiency of JDE. This should provide a practical approach in superconducting digital electronics applications.

We thank Aaron Sharpe for his critical reading of the manuscript and suggestions, and are grateful to Igor Žutić for his helpful comments. The work at Sandia is supported by the LDRD program. J.J.C., W.P., and E.R. acknowledge support from DOE, Grant No. DE-SC0022245. Device fabrication was performed at the Center for Integrated Nanotechnologies, a U.S. DOE, Office of BES, user facility. Sandia National Laboratories is a multimission laboratory managed and operated by National Technology and Engineering Solutions of Sandia LLC, a wholly owned subsidiary of Honeywell International Inc. for the U.S. DOE's National Nuclear Security Administration under contract DE-NA0003525. This paper describes objective technical results

and analysis. Any subjective views or opinions that might be expressed in the paper do not necessarily represent the views of the U.S. DOE or the United States Government.

References

- [1] Y. Zhang *et al.*, Phys. Rev. X **12**, 041013 (2022).
- [2] M. Davydova, S. Prembabu, and L. Fu, Science Advances **8**, eabo0309 (2022).
- [3] F. Ando *et al.*, Nature **584**, 373 (2020).
- [4] H. Narita *et al.*, Nature Nanotechnology **17**, 823 (2022).
- [5] K.-R. Jeon *et al.*, Nature Materials **21**, 1008 (2022).
- [6] H. Wu *et al.*, Nature **604**, 653 (2022).
- [7] J.-X. Lin *et al.*, Nature Physics **18**, 1221-1227 (2022).
- [8] M. Nadeem, M.S. Fuhrer, and X.L. Wang, Nature Reviews Physics **5**, 558 (2023).
- [9] K. Yasuda *et al.*, Nature Communications **10**, 2734 (2019).
- [10] B. Pal *et al.*, Nature Physics **18**, 1228–1233 (2022).
- [11] M. Masuko *et al.*, npj Quantum Materials **7**, 104 (2022).
- [12] N.F.Q. Yuan and L. Fu, PNAS **118**, e2019063118 (2021).
- [13] B. Pekerten *et al.*, Phys. Rev. B **105**, 054504 (2022).
- [14] Y. Tanaka, B. Lu, and N. Nagaosa, Phys. Rev. B **106**, 214524 (2022).
- [15] C.-Z. Chen *et al.*, Phys. Rev. B **98**, 075430 (2018).
- [16] A. A. Kopasov, A. G. Kutlin, and A. S. Mel'nikov, Phys. Rev. B **103**, 144520 (2021).
- [17] Y. Tokura and N. Nagaosa, Nature Communications **9**, 3740 (2018).
- [18] M. S. Anwar *et al.*, Commun Phys **6**, 290 (2023)
- [19] C. J. Trimble *et al.*, npj Quantum Materials **6**:61 (2021)
- [20] R.S. Souto, M. Leijnse, and C. Schrade, Phys. Rev. Lett. **129**, 267702 (2022)
- [21] Ya.V. Fominov and D.S. Mikhailov, Phys. Rev. B **106**, 134514 (2022).
- [22] C. Baumgartner *et al.*, Nature Nanotechnology **17**, 39–44 (2022).
- [23] Y. Miyasaka *et al.*, Applied Physics Express **14**, 073003 (2021).
- [24] T. Golod and V.M. Krasnov, Nature Communications **13**, 3658 (2022).
- [25] L. Bauriedl *et al.*, Nature Communications **13**, 4266 (2022).
- [26] J. Díez-Mérida *et al.*, Nature Communications **14**, 2396 (2023).
- [27] Y.-Y. Lyu *et al.*, Nature Communications **12**, 2703 (2021).
- [28] A. Daido, Y. Ikeda, and Y. Yanase, Phys. Rev. Lett. **128**, 037001 (2022).
- [29] N. F. Q. Yuan and L. Fu, PNAS **119**, e2119548119 (2022).
- [30] J. J. He, Y. Tanaka, and N. Nagaosa, New Journal of Physics **24**, 053014 (2022).
- [31] S. Ilić and F. S. Bergeret, Phys. Rev. Lett. **128**, 177001 (2022).
- [32] H.D. Scammell, J.I. A. Li, and M.S. Scheurer, 2D Materials **9**, 025027 (2022).
- [33] B. Zhai *et al.*, Phys. Rev. B **106**, L140505 (2022).
- [34] B. Zinkl, K. Hamamoto, and M. Sgrist, Phys. Rev. Research **4**, 033167 (2022).
- [35] H. F. Legg, D. Loss, and J. Klinovaja, Phys. Rev. B **106**, 104501 (2022).
- [36] K. Takasan, S. Sumita, and Y. Yanase, Phys. Rev. B **106**, 014508 (2022).
- [37] Y.-J. Wei *et al.*, Phys. Rev. B **106**, 165419 (2022).
- [38] R. Wakatsuki and N. Nagaosa, Phys. Rev. Lett. **121**, 026601 (2018).
- [39] R. Wakatsuki *et al.*, Science Advances **3**, e1602390 (2017).
- [40] J. Shin *et al.*, Phys. Rev. Research **5**, L022064 (2023).
- [41] T. Karabassov *et al.*, Phys. Rev. B **106**, 224509 (2022).
- [42] D. Wang, Q.-H. Wang, and C. Wu, arXiv :2209.12646
- [43] F. Paolucci, G. De Simoni, and F. Giazotto, arXiv:2211.12127
- [44] J.-X. Hu *et al.*, arXiv: 2211.14846
- [45] G.P. Mazur *et al.*, arXiv:2211.14283

- [46] Y. Zhang and Z. Wang, arXiv:2209.03520v1
- [47] J.F. Steiner *et al.*, arXiv:2212.06866.
- [48] M. Trahms *et al.*, Nature 615, 628 (2023).
- [49] R. Kealhofer *et al.*, Phys. Rev. B 107, L100504 (2023).
- [50] E. Bocquillon *et al.*, Nature Nanotechnology 12,137–143 (2017)
- [51] X. Shi *et al.*, J. of Appl. Phys. 118, 133905 (2015).
- [52] J. Hu, C. Wu, and X. Dai, Phys. Rev. Lett. **99**, 067004 (2007).
- [53] V. M. Edelstein, Phys. Rev. Lett. **75**, 2004 (1995).
- [54] P.B. Chen *et al.*, arXiv:2303.07701.
- [55] S. Ghosh *et al.*, arXiv:2210.11256.
- [56] A. Soori, Phys. Scr. 98, 065917 (2023).
- [57] P.A. Volkov *et al.*, arXiv:2307.01261
- [58] E.W. Hodt *et al.*, arXiv:2306.13124.
- [59] T.H. Kokkeler, A.A. Golubov, and F.S. Bergeret, Phys. Rev. B 106, 214504 (2022).
- [60] N. Lotfizadeh *et al.*, arXiv:2303.01902.
- [61] Y. Hou *et al.*, Phys. Rev. Lett. 131, 027001 (2023).
- [62] S.Y.F. Zhao *et al.*, Science 382, 1422 (2023).
- [63] C. Leroux *et al.*, arXiv:2209.06194
- [64] S.R. Lee *et al.*, Chem. of Mat. 31, 26 (2019).
- [65] S. M. Young *et al.*, Phys. Rev. Lett. 108, 140405 (2012).
- [66] Z. Wang *et al.*, Phys. Rev. B 88, 125427 (2013).
- [67] See Supplemental Material for detailed information.
- [68] I. Žutić *et al.*, Materials Today 22, 85 (2019).
- [69] W. Yu *et al.*, Phys. Rev. Lett. 120, 177704 (2018).
- [70] W. Yu *et al.*, Phys. Rev. Research 2, 032002(R) (2020).
- [71] N. Li et al, Supercond. Sci. Technol. 35, 044003 (2022).
- [72] A. Rashidi *et al.*, APL Mater. 11, 041117 (2023).
- [73] R. Haller *et al.*, Phys. Rev. B 108, 094514 (2023).
- [74] J. Tiira *et al.*, Nature Communications 8, 14984 (2017).
- [75] M. Weides et al, Phys. Rev. Lett. 97, 247001 (2006).
- [76] X.-Z. Yan and C.-R. Hu, Phys. Rev. Lett. 83, 1656 (1999).
- [77] S. M. Frolov *et al.*, Phys. Rev. B 74, 020503(R) (2006).
- [78] C. Ciaccia et al., Phys. Rev. Research 5, 033131 (2023).
- [79] T.A. Fulton, L.N. Dunkleberger, and R.C. Dynes, Phys. Rev. B 6, 855 (1972).
- [80] J.J. Cuozzo *et al.*, Nature Physics (2024). <https://doi.org/10.1038/s41567-024-02412-4>.
- [81] T.K. Ng and N. Nagaosa, EPL 87, 17003 (2009).
- [82] J.J. Cuozzo et al, under preparation.
- [83] J.J. Cuozzo *et al.*, Phys. Rev. Research 6, 023011 (2024).
- [84] M. N. Ali *et al.*, Inorganic Chemistry 53, 4062 (2014).
- [85] W. Yu et al., Nanotechnology 33, 415002 (2022)
- [86] E. Zhang *et al.*, Nano Letters 21, 288 (2021).
- [87] R. Córdoba *et al.*, Nature Communications 4, 1437 (2013).

Figure1:

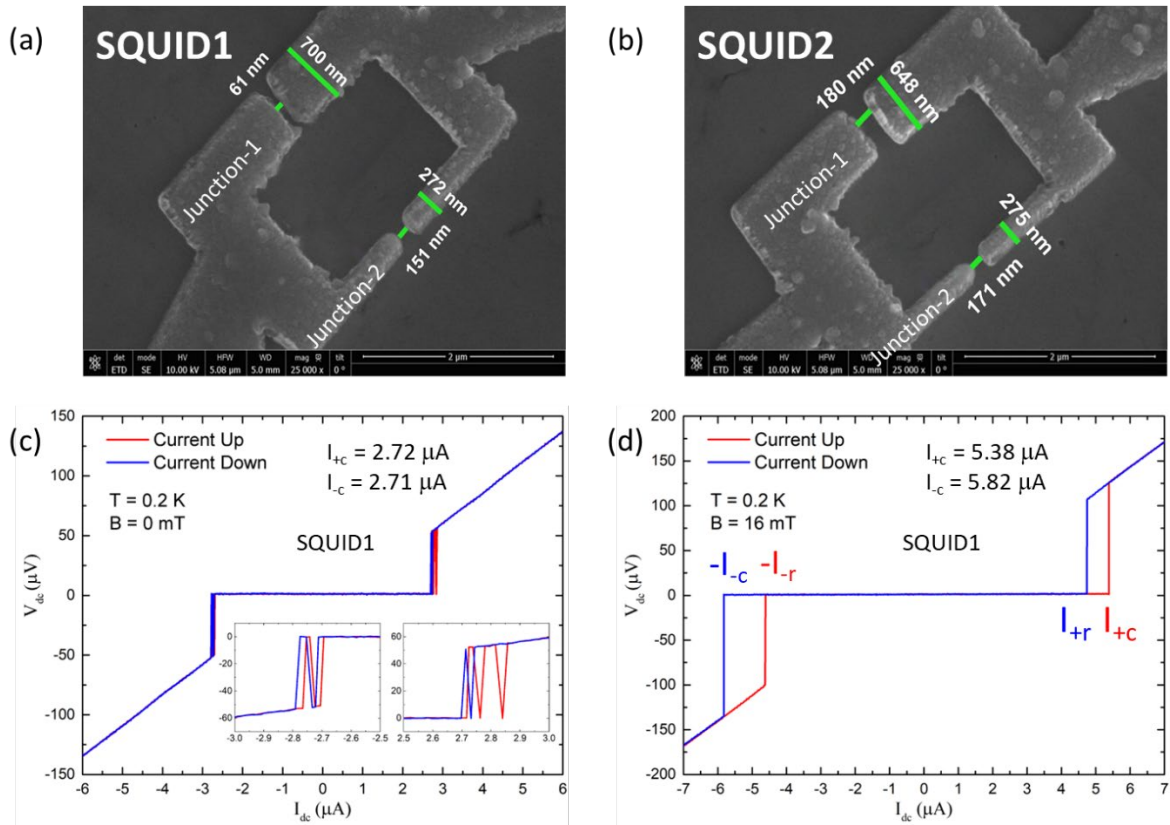


Fig. 1: Asymmetric superconducting quantum interference devices and the I-V characterizations. (a) and (b) SEM images of the two asymmetric SQUIDs studied. The black background represents Cd_3As_2 thin flakes. (c) Current-voltage (I - V) characteristics in SQUID1 at zero magnetic field $B = 0$. Multiple switching behaviors are observed in the critical and retrapping currents, see the bottom right inset. (d) I - V characteristics in SQUID1 at $B = 16$ mT. The position of I_{+c} , $-I_c$, I_{+r} and $-I_r$ are marked. Herein, all four currents I_{+c} , I_c , I_{+r} , and I_r are taken positive.

Figure 2:

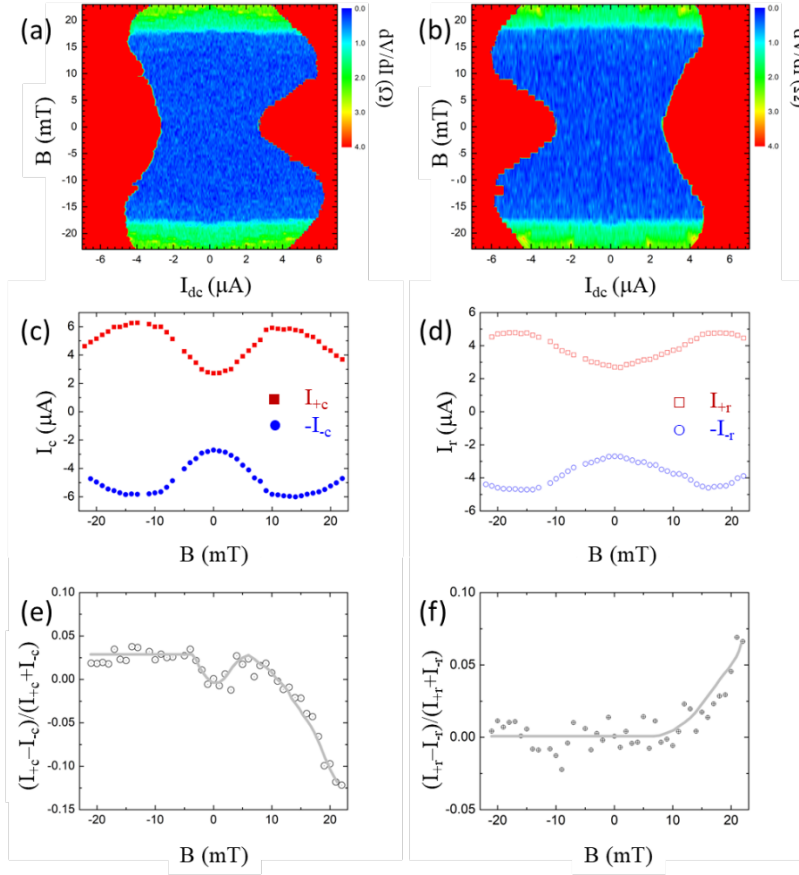


Fig. 2. Magnetic field induced JDE in SQUID1. (a) and (b) Differential resistance dV/dI as a function of DC current and B fields for two current sweeping directions. I_{+c} and $-I_{-c}$, and the efficiency $\eta_c = (I_{+c}-I_{-c})/(I_{+c}+I_{-c})$ as a function of B field are shown in (c) and (e), respectively. I_{+r} and $-I_{-r}$ (d) and $\eta_r = (I_{+r}-I_{-r})/(I_{+r}+I_{-r})$ (f) as a function of B field. The gray lines are a guide to the eye.

Figure 3:

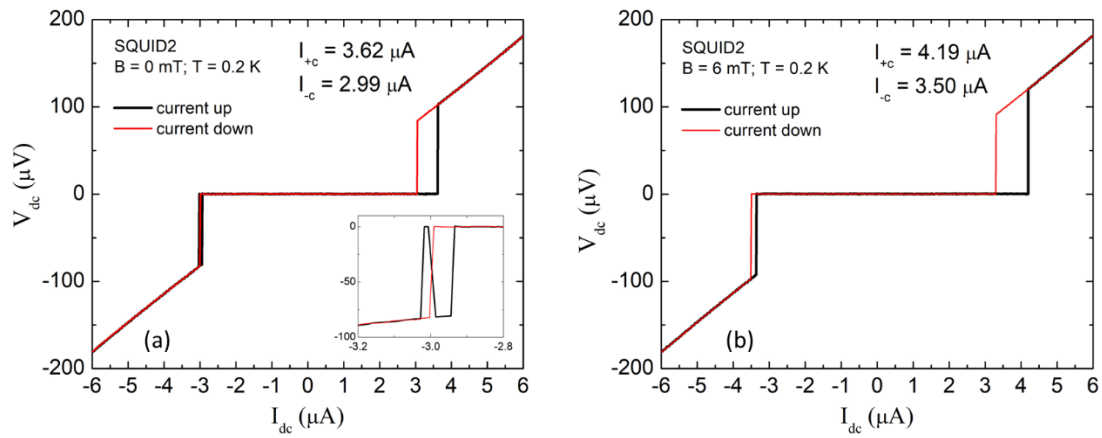


Fig. 3 Zero-magnetic field JDE in SQUID2. (a) I-V characteristics in SQUID2 at zero magnetic field. A large JDE is seen. $I_{+c} = 3.62$ μA and $I_{-c} = 2.99$ μA . This large JDE remains strong at a finite magnetic field of $B = 6$ mT (b).

Figure 4:

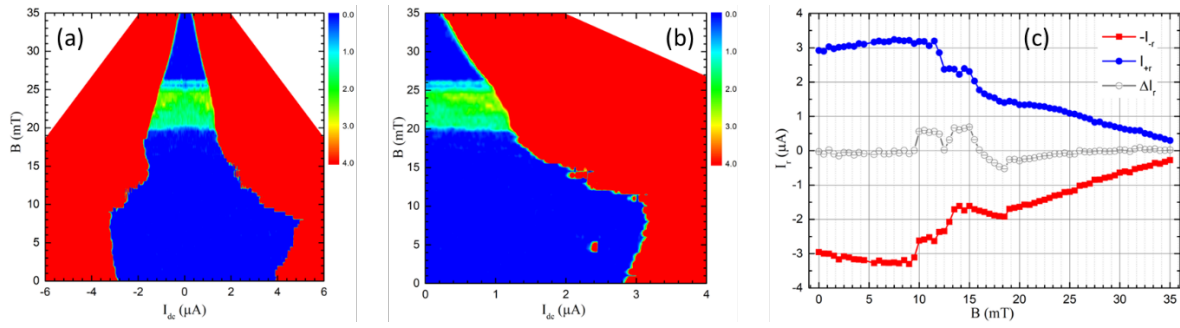


Fig.4. JDE of retrapping currents in SQUID2. (a) and (b) dV/dI as a function of DC current and magnetic field for two current sweeping directions. (c) I_{+r} , $-I_{-r}$, and ΔI_r as a function of B field.

Figure 5:

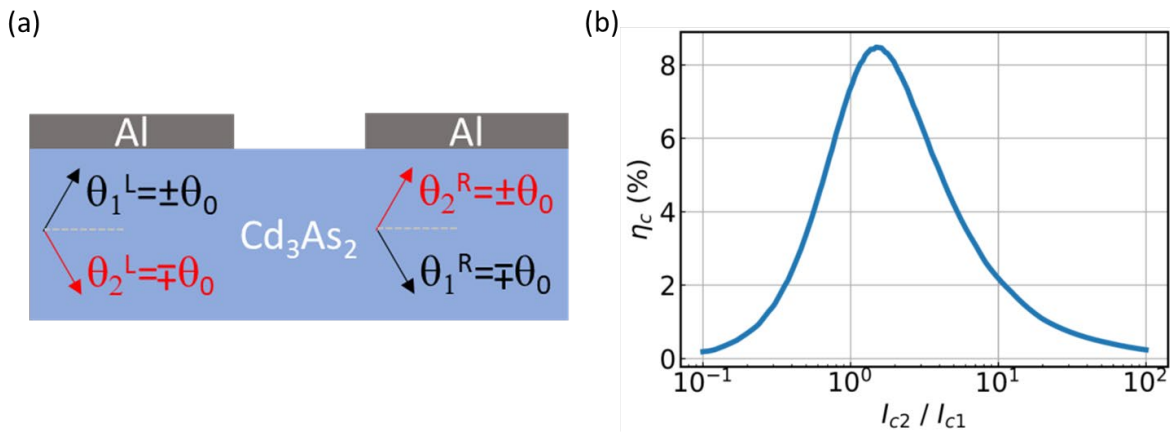


Fig. 5 Theoretical analysis. (a) Schematic representation of equilibrium phases of order parameters in a two-band superconductor Josephson junction. (b) Simulations of the efficiency (η_c) of JDE vs. the ratio of the critical currents in the two Josephson junction arms in an asymmetric SQUID.